

# Simultaneous measurement of multimode squeezing

ISMAIL BARAKAT,<sup>1,†,\*</sup> MAHMOUD KALASH,<sup>1,2,†</sup> DENNIS SCHARWALD,<sup>3</sup> POLINA SHARAPOVA,<sup>3</sup> NORBERT LINDLEIN,<sup>1</sup> MARIA CHEKHOVA<sup>1,2</sup>

<sup>1</sup>*Friedrich-Alexander-Universität Erlangen-Nürnberg, Staudtstr. 7/B2, 91058 Erlangen, Germany*

<sup>2</sup>*Max-Planck Institute for the Science of Light, Staudtstr. 2, Erlangen D-91058, Germany*

<sup>3</sup>*Paderborn University, Department of Physics, Warburger Straße 100, D-33098 Paderborn, Germany*

\*Corresponding author: [ismail.barakat@fau.de](mailto:ismail.barakat@fau.de)

† These authors contributed equally

## Abstract:

Multimode squeezed light is an increasingly popular tool in photonic quantum technologies, including sensing, imaging, and computation. Meanwhile, the existing methods of its characterization are technically complicated, and in the best case, deal with a single mode at a time. Here, we demonstrate experimentally how the squeezing can be measured in multiple spatial modes simultaneously, using optical parametric amplification and direct detection followed by modal decomposition based on spatial intensity correlations. We apply this method to a multimode squeezed vacuum generated via high-gain parametric down-conversion. We measure the degrees of squeezing and anti-squeezing for eight strongest spatial modes, obtaining highest squeezing and anti-squeezing values of  $-5.2 \pm 0.2$  dB and  $8.6 \pm 0.3$  dB, respectively. A similar method can be applied to characterize the frequency modes.

## 1. Introduction

Squeezed light plays a key role in photonic quantum technologies [1]. In metrology, it provides the measurement of the phase beyond the classical sensitivity limit [2]; its use in gravitational-wave detectors was crucial for the first observation of gravitational waves [3, 4]. Squeezed light enhances signal-to-noise ratio in Raman spectroscopy [5], as well as in imaging [6] and microscopy [7, 8]. Noteworthy, imaging and spectroscopy applications require squeezed light that is multimode in space/angle and time/frequency, respectively. Multiple squeezed modes are also needed in continuous-variable quantum information processing and quantum communication, where each mode serves as an information carrier [9] and a large set of modes can be used for measurement-based quantum computation [10–12].

Therefore, an important task is to characterize squeezing in multiple spatial and temporal modes. The standard way to measure squeezing is through homodyne detection, where the squeezed light is overlapped with a strong coherent beam, called the local oscillator, which matches its frequency and angular spectrum. But in the case of multimode squeezed light, each mode requires an individually shaped local oscillator. In practice, this means that different modes are characterized one by one, with the local oscillator shaped differently each time [9, 13]. It is also possible to characterize a certain mode after filtering it from the rest; but because squeezing is easily destroyed by loss, the filtering has to be projective. Although a Gaussian spatial mode can be indeed filtered out losslessly using a single-mode fiber [14], filtering of higher-order spatial modes requires more complicated methods to minimize losses [15–17]. It is even more difficult to perform projective filtering of a frequency mode: the only existing method is through nonlinear frequency conversion [18]. However, none of these methods allows the characterization of all modes simultaneously.

Recently, it was shown that squeezing can be measured via direct detection using optical parametric amplification [19–22]. Indeed, the mean number of photons at the output of a phase-sensitive optical parametric amplifier (OPA) amplifying a generalized quadrature  $\hat{Q}_\phi$  and

de-amplifying the conjugated quadrature  $\hat{P}_\phi$ , defined at the optical phase  $\phi$  [23], is

$$\langle \hat{N}_\phi \rangle = e^{2G} \langle \hat{Q}_\phi^2 \rangle + e^{-2G} \langle \hat{P}_\phi^2 \rangle - \frac{1}{2}, \quad (1)$$

where  $G$  is the amplification gain. If the amplification is sufficiently strong and the input state has  $\langle \hat{Q}_\phi \rangle = 0$ , the output mean photon number becomes

$$\langle \hat{N}_\phi \rangle = e^{2G} \Delta Q_\phi^2, \quad (2)$$

where  $\Delta Q_\phi^2$  is the input quadrature variance. In other words, high-gain phase-sensitive amplification maps the variance of an input quadrature to the output mean photon number, or mean intensity. The quadrature that gets amplified can be selected by scanning the phase of the OPA pump. To find out whether the quadrature is squeezed, its variance is compared to the vacuum noise level, the latter can be obtained by amplifying the vacuum, i.e., blocking the amplifier input.

This method of squeezing measurement offers three primary advantages. Firstly, it can operate with multiple input broadband modes simultaneously, provided the parametric amplifier is multimode and its modes align with the input modes. Secondly, it is tolerant to detection losses and, as long as the amplification is strong enough, also to detection noise [24]. Lastly, this method employs direct detection, which is technically simpler than homodyne detection.

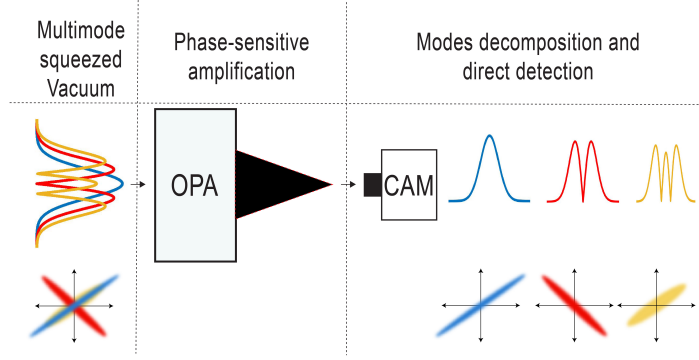


Fig. 1. Generalized and simplified scheme of measuring multimode squeezing through phase-sensitive optical parametric amplification.

In this work, we combine these advantages with a method we developed to reconstruct the shapes and weights of the eigenmodes of an OPA, both in the frequency [25] and spatial [26] domains. The method is based on the fact that the Schmidt modes (also known as squeezing modes [27], broadband modes [28], or supermodes [29]) of the signal and idler beams of an OPA coincide with the coherent modes of only one (signal or idler) beams taken separately [30]. Furthermore, given that each mode exists in a thermal state, the modal decomposition can be reconstructed by measuring the covariance of intensities at the OPA output. The measured weights define the mean photon numbers in these modes. According to Eq. (2), if the OPA modes are seeded with squeezed vacuum, these weights also define the squeezing levels.

Figure 1 illustrates the general scheme of our method. A multimode quantum state, where each mode  $m$  exhibits zero mean quadratures,  $\langle \hat{Q}_m \rangle = \langle \hat{P}_m \rangle = 0$ , is directed to a multimode OPA that aligns with the input mode structure. By changing the OPA pump phase, we scan the phase  $\phi$  of the amplified quadrature simultaneously across all modes. Subsequently, an ensemble of far-field intensity distributions is measured at the output, from which the mean photon number of each spatial mode is extracted.

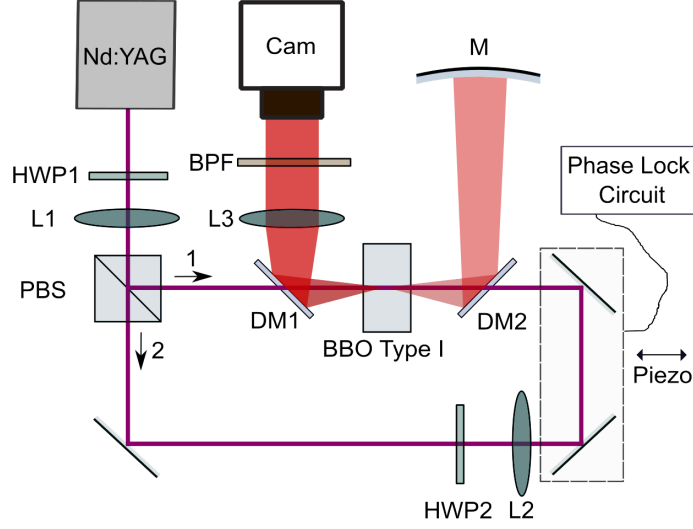


Fig. 2. Experimental setup. Polarizing beam splitter PBS splits the pump into two arms of a Sagnac-like interferometer, the splitting ratio being controlled by half-wave plate HWP1. Reflected beam 1, focused by lens L1, pumps a BBO crystal (squeezer) to generate multimode SV. The SV is then reflected by dichroic mirror DM2, imaged by spherical mirror M back into the same crystal, which now plays the role of the OPA and amplifies the SV. The amplifier is pumped by transmitted beam 2, which is focused by lenses L1 and L2 and whose polarization is controlled by HWP2. After amplification, SV is separated from the pump by dichroic mirror DM1, filtered by band-pass filter BPF, and detected by a camera in the Fourier plane of lens L3.

## 2. Experimental setup

Figure 2 shows the experimental setup. The third harmonic of a pulsed Nd:YAG laser at 354.6 nm (pulse width 18 ps, repetition rate 1 kHz, average power 45 mW) is focused by lens L1 and split by a polarizing beam splitter (PBS) between the two arms of a Sagnac-like interferometer, a half-wave plate (HWP1) controlling the splitting ratio. A single 3 mm beta-barium borate (BBO) crystal, cut for type-I collinear frequency-degenerate parametric down-conversion (PDC), is placed into the pump beam waist and serves a dual purpose. First, it is a squeezer; it generates multimode squeezed vacuum (SV) from the pump reflected by the PBS (beam 1) and focused into a waist of  $w = 70 \mu\text{m}$ , the squeezing parameter for collinear emission being  $G_1 = 1 \pm 0.3$ . Second, it plays the role of the OPA (amplifier); it amplifies/de-amplifies the SV as the latter is separated from the pump by dichroic mirror DM2 and reflected back by spherical mirror M. The amplifier, with the parametric gain  $G_2 = 4.0 \pm 0.4$  for the collinear direction, is pumped by beam 2, transmitted through the PBS. The polarization of the beam is corrected by half-wave plate HWP2 and its waist is imaged onto the OPA by lens L2. The spherical mirror plays an important role: it images the SV back into the BBO crystal, ensuring that all spatial modes undergo phase-sensitive amplification with the same phase [20]. Whether amplification or de-amplification occurs, is determined by the phase of the pump, which is controlled with a piezoelectric actuator affixed to a translation stage. For more details of the experimental setup.

After undergoing phase-sensitive amplification, the multimode SV is reflected by dichroic mirror DM1 and filtered by band-pass filter BPF with 10 nm bandwidth centred around the degenerate wavelength. This filtered SV is then detected by a gated and cooled sCMOS camera with 55% quantum efficiency, positioned at the Fourier plane of lens L3. The camera records 2D

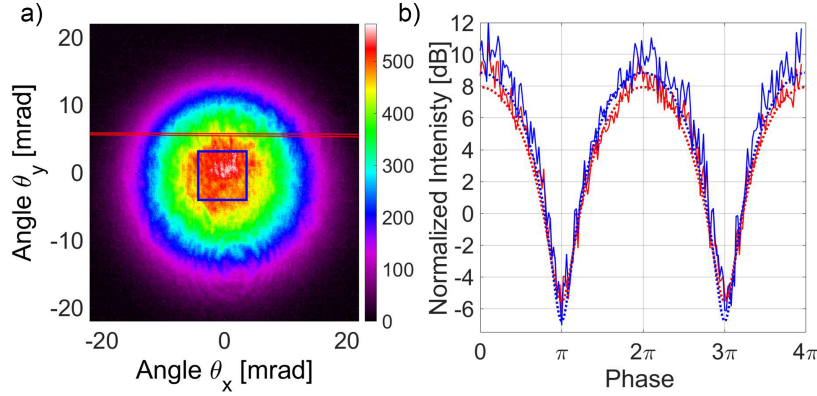


Fig. 3. (a) Far-field intensity distribution at the amplifier output. The blue square and the red stripe indicate the areas used for measuring squeezing in the collinearly emitted squeezed vacuum (SV) and for spatial modes reconstruction, respectively. (b) The intensities at the amplifier output integrated over the blue square (blue trace) and the red stripe (red trace) in panel (a), normalized to their values in the case of vacuum at the input, plotted against the amplification phase. The minima (maxima) indicate the degree of squeezing (anti-squeezing). Dotted lines show the results of theoretical calculations.

intensity distributions.

Figure 3(a) displays the distribution obtained by averaging over 1500 pulses. We align the spherical mirror so that while scanning the phase of the propagating pump beam in the second arm, the intensity distribution oscillates as a whole [20]. This procedure is aimed at balancing the phases of all spatial modes so that the condition for both amplification and de-amplification is met concurrently across all modes. To demonstrate squeezing for the collinearly emitted SV (Fig. 3(b)), we integrate the signal over the central area of the camera (the blue square in Fig. 3(a)). This integrated signal is then normalized to the signal measured when the radiation of the squeezer is blocked, allowing the OPA to amplify solely the vacuum. The measurement shows a visibility of  $96 \pm 1\%$  and the degrees of squeezing and anti-squeezing of  $-6.0 \pm 0.6$  dB and  $10 \pm 1$  dB, respectively.

Further, we acquire three separate sets of single-pulse frames; the first, with the phase locked at the ‘bright fringe’, corresponding to the maximum of the interferogram in Fig. 3(b) and to the case where the anti-squeezed quadrature is amplified; the second, with the phase locked at the ‘dark fringe’, (the squeezed quadrature is amplified), corresponding to the minimum of the interferogram, and the third, for the amplified vacuum. Each dataset comprises 1500 frames and is further used to extract the shapes of the spatial eigenmodes along with their weights. Together with the integral mean intensity, these weights determine the numbers of photons in each mode after the OPA.

### 3. Schmidt modes reconstruction

The Schmidt modes of a SV are those minimizing the number of correlations between its signal and idler subsystems [31]. In other words, a single Schmidt mode of the signal beam has photon-number correlations with only a single Schmidt mode of the idler beam. In particular, the Schmidt modes of type-I collinear degenerate PDC very closely resemble the Hermite-Gauss modes of paraxial beams [30, 32]. Although these modes are two-dimensional and can be represented as functions of both  $\theta_x$  and  $\theta_y$  angles in the far field, for type-I collinear PDC, they can be considered, to a good approximation, as factorable:  $u_{mn}(\theta_x, \theta_y) = u_m(\theta_x)u_n(\theta_y)$  [30, 32].

For simplicity, we focus solely on one-dimensional modes  $u_m(\theta_x)$ . To find them, we rely on their identity with the coherent modes of one subsystem, signal or idler [30, 33]. Therefore, we filter out one subsystem by considering only the upper segment of the far-field intensity distribution depicted in Fig. 3 (a). This selection serves to eliminate the signal-idler correlations.

To reconstruct the modes, we obtain a one-dimensional intensity distribution by selecting a stripe covering the  $\theta_y$  values from  $\theta_1 = 6.5$  mrad to  $\theta_2 = 7.5$  mrad (shown in Fig. 3 (a) by red lines) and integrating over  $\theta_y$ :  $I(\theta_x) \equiv \int_{\theta_1}^{\theta_2} I(\theta_x, \theta_y) d\theta_y$ . For this one-dimensional intensity distribution, we measure the intensity covariance,

$$\text{Cov}(\theta_x, \theta'_x) = \langle I(\theta_x) I(\theta'_x) \rangle - \langle I(\theta_x) \rangle \langle I(\theta'_x) \rangle. \quad (3)$$

The resulting normalized covariance distribution  $C(\theta_x, \theta'_x) = \text{Cov}(\theta_x, \theta'_x) / \int d\theta_x d\theta'_x \text{Cov}(\theta_x, \theta'_x)$  shows the spatial auto-correlations in the signal beam [30], see the left panels of Fig. 4. Different panels show the cases corresponding to the amplification of the anti-squeezed (a, ‘bright fringe’) and squeezed (c, ‘dark fringe’) quadratures of the SV, and the vacuum amplification (b). In all cases, the covariance distribution contains the modes of only the signal subsystem.

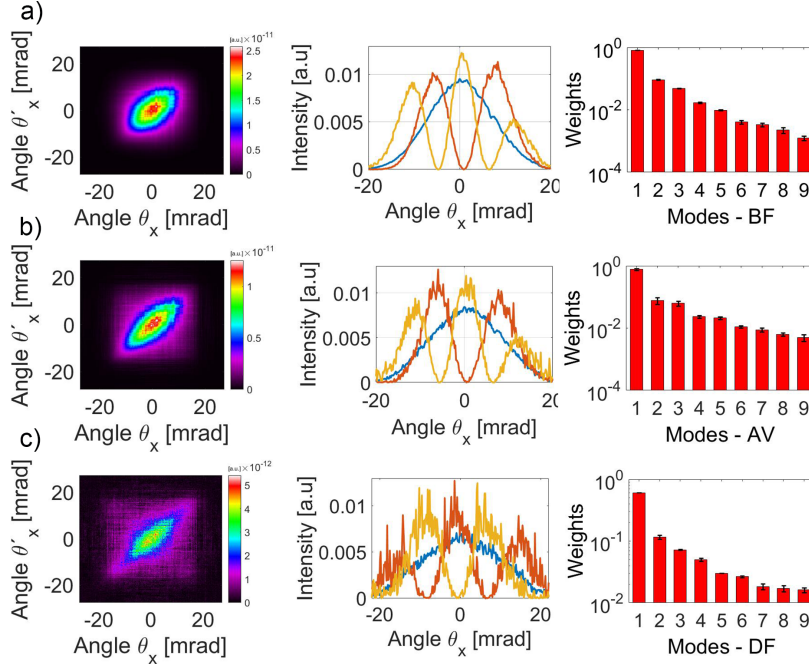


Fig. 4. From left to right: the normalized covariance  $C(\theta_x, \theta'_x)$ , the normalized intensity distributions of the three lowest-order modes, and the weights of the modes for the cases where OPA amplifies the anti-squeezed quadrature of the SV (‘bright fringe’, a), the vacuum (b), and the squeezed quadrature of the SV (‘dark fringe’, c).

As shown in Refs. [26, 33], the normalized covariance can be written as a squared coherent-mode decomposition,

$$C(\theta_x, \theta'_x) = \left[ \sum_m \lambda_m u_m(\theta_x) u_m^*(\theta'_x) \right]^2, \quad (4)$$

where  $\lambda_m$  are the eigenvalues (weights) of the modes, satisfying the normalization condition  $\sum_m \lambda_m = 1$ . These weights determine the populations  $\langle \hat{N}_m \rangle$  of different modes relative to the

total mean photon number  $\langle \hat{N}_{tot} \rangle$  [14],

$$\langle \hat{N}_m \rangle = \lambda_m \langle \hat{N}_{tot} \rangle. \quad (5)$$

Applying the singular-value decomposition (SVD) to the square root of the normalized covariance distribution yields the weights and shapes of the modes. The middle panels of Fig. 4 show the intensity distributions of the three strongest modes,  $|u_m(\theta_x)|^2$ , while the right-hand panels a,b,c depict the mode weights  $\lambda_m^B$ ,  $\lambda_m^{AV}$ , and  $\lambda_m^D$  for the bright fringe, amplified vacuum, and dark fringe, respectively. Furthermore, we restrict our analysis to 12 modes, as the reconstruction becomes increasingly noisy for higher-order modes. Accordingly, the normalization condition is applied to  $\lambda_m$  with  $1 \leq m \leq 12$ .

The weights of the modes decrease with the order  $m$ , as expected for a type-I collinear degenerate PDC [32]. The Schmidt number, i.e., the effective number of modes, defined as  $K = \frac{1}{\sum_m \lambda_m^2}$ , is  $2.6 \pm 0.5$  for the dark fringe,  $1.8 \pm 0.2$  for the amplified vacuum, and  $1.4 \pm 0.1$  for the bright fringe. Indeed, as the brightness of an OPA output increases, its effective number of populated modes decreases [35]. Nevertheless, even for the bright fringe, at least first eight modes are sufficiently populated to be characterized.

So far, we assumed that the Schmidt modes of the squeezer coincide with those of the whole two-crystal interferometer, which are reconstructed at the output. However, this is not necessarily the case. Even if the parameters of the squeezer and the OPA (specifically the length and the pump beam waist,) are the same, their mode shapes are different: the mode widths depend on the parametric gain and  $G_1 < G_2$ . Therefore, in the general case, each mode of the squeezer has a nonzero overlap with all modes of the OPA, as well as of the whole two-crystal interferometer, whose effective gain values are  $G_1 + G_2$  for the bright fringe and  $G_2 - G_1$  for the dark fringe. This is why, to determine the degree of squeezing for a specific squeezer mode, one needs the weights of several (ideally, all) modes of the interferometer. It should be noted that the difference in sizes between the modes of the interferometer output for different cases (dark fringe, amplified vacuum, bright fringe) is not significant, as we can see in the middle panels of Fig. 4. This is because the corresponding effective gain values ( $G_2 - G_1 = 3, G_2 = 4, G_2 + G_1 = 5$ ) are close. However, the mode sizes of the squeezer are significantly different from those of both the amplifier and the interferometer.

If we denote the modes of the squeezer as  $v_l(\theta_x)$  and the input modes of the amplifier as  $w_n(\theta_x)$ , their overlap is given by the matrix  $g_{ln} = \int d\theta_x [v_l(\theta_x)]^* w_n(\theta_x)$ . Figure 5a shows this matrix, calculated numerically with the use of the experimental parameters (measurement of shapes  $v_l(\theta_x)$  is impossible because of the weak signal for a gain of  $G_1 = 1$ ). The ‘checkerboard’ structure arises from the zero overlap between odd and even modes, which are even and odd functions of  $\theta_x$ , respectively. This pattern holds for modes up to order 9, however, for modes of higher orders, this structure is violated.

Noteworthy, it is possible to make the overlap matrix  $g_{ln}$  nearly diagonal by focusing the pump beams in the squeezer and the amplifier differently. In the amplifier, whose gain is higher than that of the squeezer, the modes are broader. However, their angular profiles can be reduced by increasing the pump beam waist.

Meanwhile, the overlap between the amplifier output modes  $u_n^{amp}(\theta)$  and the output modes of the two-crystal interferometer  $u_k(\theta)$  is given by the matrix  $h_{nk} = \int d\theta [u_n^{amp}(\theta)]^* u_k(\theta)$ , with the normalization condition  $\sum_n |h_{ln}|^2 = \sum_l |h_{ln}|^2 = 1$  (Fig. 5b). As expected, the  $h_{ln}$  matrix is nearly diagonal; therefore, further on we assume  $h_{ln} = \delta_{ln}$ , where  $\delta_{ln}$  is the Kronecker symbol.

#### 4. Multimode squeezing measurement

The multimode amplifier transforms each output mode of the squeezer into a set of modes at the output of the interferometer. Denoting the photon annihilation and creation operators of the

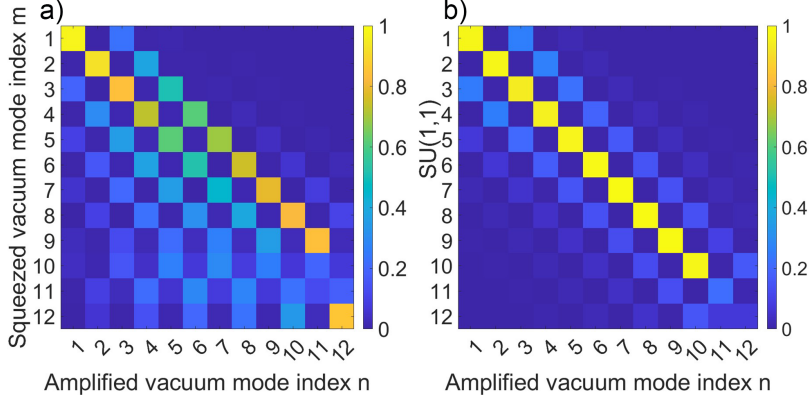


Fig. 5. The overlap coefficients: (a)  $g_{ln}$  between the modes of the squeezer and the input modes of the amplifier and (b)  $h_{ln}$  between the modes of the amplifier output and the whole interferometer in the bright fringe.

squeezer output modes as  $\hat{A}_l, \hat{A}_l^\dagger$  and of the interferometer output modes as  $\hat{A}_n^{\text{int,out}}, [\hat{A}_n^{\text{int,out}}]^\dagger$ , with  $l, n$  numbering the modes (see the Appendix), we write the inverse multimode Bogoliubov transformation (23) as

$$\hat{A}_l = \sum_n g_{ln} \left[ \sqrt{\Lambda_n + 1} \hat{A}_n^{\text{int,out}} \mp \sqrt{\Lambda_n} [\hat{A}_n^{\text{int,out}}]^\dagger \right], \quad (6)$$

where we assumed the  $h_{nk}$  matrix to be diagonal and  $\Lambda_n = \sinh^2(r_n)$ , with  $r_n$  being the parametric gain for mode  $n$  of the amplifier, is the photon number in mode  $n$  of the amplified vacuum. The minus sign here corresponds to the bright fringe, and the plus sign, to the dark fringe.

From this relation, we can express the position  $\hat{Q}_l$  and momentum  $\hat{P}_l$  operators of the squeezer mode  $l$  in terms of the position and momentum operators  $\hat{Q}_n^{\text{int,out}}, \hat{P}_n^{\text{int,out}}$  of the interferometer output modes  $n$ . We assume, without the loss of generality, that  $\hat{Q}_l$  are anti-squeezed while  $\hat{P}_l$  are squeezed.

Denoting the output position quadratures for the bright and dark fringes as  $\hat{Q}_n^{\text{B}}$  and  $\hat{Q}_n^{\text{D}}$ , respectively, and similarly for the momentum quadratures, we obtain

$$\begin{aligned} \hat{Q}_l &= \sum_n \left[ \text{Re}[M_{ln}^{-/+}] \hat{Q}_n^{\text{B/D}} - \text{Im}[M_{ln}^{-/+}] \hat{P}_n^{\text{B/D}} \right], \\ \hat{P}_l &= \sum_n \left[ \text{Im}[M_{ln}^{+/-}] \hat{Q}_n^{\text{B/D}} + \text{Re}[M_{ln}^{+/-}] \hat{P}_n^{\text{B/D}} \right], \end{aligned} \quad (7)$$

where we introduced the matrices  $M_{ln}^{-/+} = g_{ln} \sqrt{\Lambda_n + 1} \mp g_{ln}^* \sqrt{\Lambda_n}$ .

We align the spherical mirror so that the intensity distribution at the interferometer output (Fig. 3a) oscillates as a whole, with the intensity at each point being minimal for the dark fringe and maximal for the bright fringe. This means that for each mode, the position quadrature (already anti-squeezed, i.e., amplified) is further amplified in the bright fringe and de-amplified in the dark fringe, while the momentum (squeezed) quadrature behaves oppositely: it is amplified in the dark fringe and de-amplified in the bright fringe. This condition means that for each mode  $l$ , in the bright fringe the amplified quadratures ( $\hat{Q}_n^{\text{B}}$ ) get input only from quadratures  $\hat{Q}_l$ , while in the dark fringe, the amplified quadratures ( $\hat{P}_n^{\text{D}}$ ) get input only from quadratures  $\hat{P}_l$ . It is achieved when  $\text{Im}[M_{ln}^+] = \text{Im}[M_{ln}^-] = 0$ .

As a result, the alignment procedure balances the phases of the modes, ensuring that the  $g_{ln}$  matrix is real. Consequently, Eqs. (7) lead to simple relations between the position and



momentum quadratures of mode  $l$  of the squeezed vacuum (which are anti-squeezed and squeezed, respectively) and the position and momentum quadratures of all modes at the interferometer output:

$$\hat{Q}_l = \sum_n g_{ln}(\sqrt{\Lambda_n + 1} \mp \sqrt{\Lambda_n})\hat{Q}_n^{B/D}, \quad \hat{P}_l = \sum_n g_{ln}(\sqrt{\Lambda_n + 1} \pm \sqrt{\Lambda_n})\hat{P}_n^{B/D}. \quad (8)$$

Taking into account the absence of correlations between the quadratures of different Schmidt modes, we obtain from Eqs. (8) the variances of the anti-squeezed and squeezed quadratures in each mode:

$$\Delta Q_l^2 = \sum_n g_{ln}^2(\sqrt{\Lambda_n + 1} - \sqrt{\Lambda_n})^2 \langle N_n^B \rangle, \quad \Delta P_l^2 = \sum_n g_{ln}^2(\sqrt{\Lambda_n + 1} - \sqrt{\Lambda_n})^2 \langle N_n^D \rangle. \quad (9)$$

Here, we used the main principle of the method: the mean output photon numbers in different modes,  $\langle N_n^{\text{out}} \rangle$ , see also the SI. According to Fig. S1 of the SI, in the bright fringe  $\langle N_n^B \rangle = \langle (Q_n^B)^2 \rangle$ , while in the dark fringe,  $\langle N_n^D \rangle = \langle (P_n^D)^2 \rangle$ .

Meanwhile, for each vacuum mode, equations similar to (8) and (9) can be written:

$$\hat{Q}_{vac} = (\sqrt{\Lambda_n + 1} - \sqrt{\Lambda_n})\hat{Q}_n^{AV}, \quad \Delta Q_{vac}^2 = (\sqrt{\Lambda_n + 1} - \sqrt{\Lambda_n})^2 \langle N_n^{AV} \rangle, \quad (10)$$

where  $\langle N_n^{AV} \rangle = \langle (Q_n^{AV})^2 \rangle$  is the mean number of photons in the  $n$ th mode of the amplified vacuum.

Finally, we get

$$\Delta Q_l^2 = \Delta Q_{vac}^2 \sum_n g_{ln}^2 \frac{\langle N_n^B \rangle}{\langle N_n^{AV} \rangle}, \quad \Delta P_l^2 = \Delta Q_{vac}^2 \sum_n g_{ln}^2 \frac{\langle N_n^D \rangle}{\langle N_n^{AV} \rangle}. \quad (11)$$

Applying Eq. (5) to all three cases (bright fringe, amplified vacuum, dark fringe), we obtain the degrees of anti-squeezing  $AS_l$  and squeezing  $S_l$  in each mode in terms of the calculated overlap coefficients  $g_{ln}$ , measured mean total number of photons  $\langle N_{tot}^B \rangle$ ,  $\langle N_{tot}^{AV} \rangle$ ,  $\langle N_{tot}^D \rangle$  and mode weights  $\lambda_n^B, \lambda_n^{AV}, \lambda_n^D$  for the bright fringe, amplified vacuum, and dark fringe, respectively:

$$AS_l = 10 \log_{10} \sum_n g_{ln}^2 \left[ \frac{\lambda_n^B \langle N_{tot}^B \rangle}{\lambda_n^{AV} \langle N_{tot}^{AV} \rangle} \right], \quad S_l = 10 \log_{10} \sum_n g_{ln}^2 \left[ \frac{\lambda_n^D \langle N_{tot}^D \rangle}{\lambda_n^{AV} \langle N_{tot}^{AV} \rangle} \right]. \quad (12)$$

Figure 6 shows the degrees of squeezing (left) and anti-squeezing (right) measured for eight strongest modes. Both the mean values and the uncertainties were obtained by analyzing four different sets of data. The highest values are measured for the first mode, with  $-5.2 \pm 0.2$  dB squeezing and  $8.5 \pm 0.3$  dB anti-squeezing. These values agree well with the ones theoretically calculated for the output of the squeezer, assuming a parametric gain of  $G = 1.0$  and the overall losses, including those caused by imperfect alignment, amounting to 10%. The theoretical values of squeezing and antisqueezing for the same modes are represented, for convenience, by black dashed curves. The large uncertainty in the squeezing values for the highest-order modes is caused by the low level of the measured signal in the dark fringe and, as a consequence, by the inaccurate reconstruction of the modes shapes and weights. Characterization of higher-order modes is impossible, both for this reason and also because the parametric amplification for those modes is insufficiently strong to allow the simplified relation (2).

## 5. Conclusion

We have proposed and demonstrated a simple and efficient method to characterize multimode squeezed light. Our approach uses multimode optical parametric amplification followed by direct



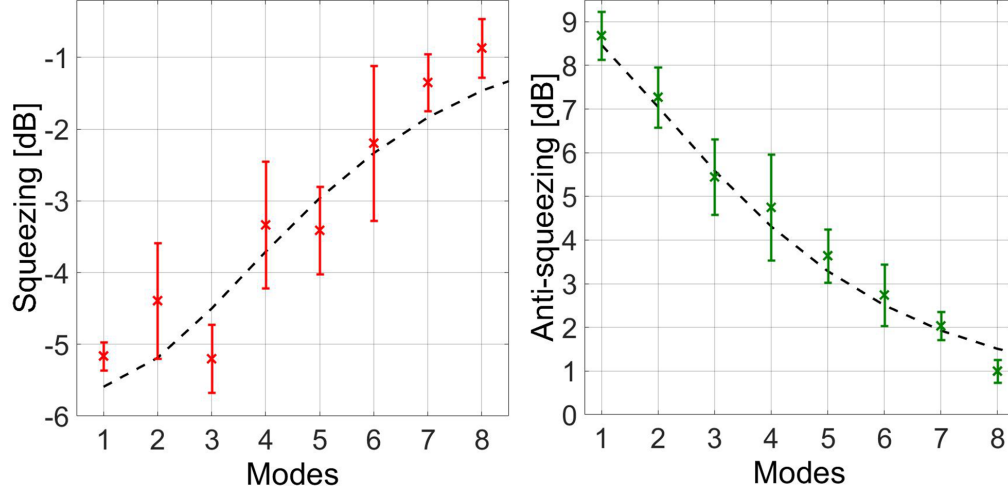


Fig. 6. The degrees of squeezing (left) and anti-squeezing (right), measured (red and green points, respectively) and calculated (dashed black line).

detection and mode weights reconstruction based on intensity correlations. In this method, all modes are measured at once without the need for filtering any of them, unlike in the commonly used homodyne detection. In addition, the method is tolerant to the detection inefficiencies. As a proof of principle, we measured squeezing and anti-squeezing for eight strongest spatial modes of squeezed vacuum generated in a traveling-wave optical parametric amplifier (‘squeezer’). We obtained the maximal values of squeezing and anti-squeezing of  $-5.2 \pm 0.2$  dB and  $8.6 \pm 0.3$  dB, respectively.

The results are in a good agreement with theoretical predictions despite the imperfect overlap between the modes of the squeezer and the modes of the amplifier, caused by their different gain values. We account for the partial mode overlap by calculating it theoretically. This task is considerably simplified due to the absence of relative phases between different modes, achieved by imaging the near field of the squeezer on the near field of the amplifier [20]. But the mode overlap between the squeezer and the amplifier can be made nearly perfect by specially designing the waists of their pump beams.

For higher-order modes, our method is not applicable for several reasons: the invalidity of the high-gain condition of the amplifier, the low contributions of high-order modes into the overall intensity, leading to the impossibility to accurately balance their phases in experiment, and a high noise in their reconstruction, especially for the dark fringe. This method can be easily extended to two-dimensional spatial modes as we showed in Ref. [30]; in this case, signal-idler correlations should be eliminated by filtering a spectral band shifted from the degenerate wavelength. The method can be generalized to frequency modes and even mode combinations, to obtain and characterize cluster states for measurement-based quantum computation [12]. The realized method would definitely assist numerous experiments on sub-shot-noise imaging and sensing.

## 6. Appendix: Schmidt modes of the OPAs

Our theoretical description is based on solving systems of integro-differential equations for each crystal separately and for the entire system, forming an  $SU(1,1)$  interferometer. In this approach, the input-output relations (Bogoliubov transformations) for the plane-wave operators can be

written as [36, 37]:

$$\hat{a}^{\text{out}}(\theta) = \int d\theta' \eta(\theta, \theta') \hat{a}(\theta') + \int d\theta' \beta(\theta, \theta') [\hat{a}^{\text{in}}(\theta')]^\dagger. \quad (13)$$

Here, the transfer functions  $\eta$  and  $\beta$  can be decomposed using the joint Schmidt decomposition (Bloch-Messiah reduction) [30, 34]:

$$\beta(\theta, \theta') = \sum_n \sqrt{\tilde{\Lambda}_n} u_n(\theta) w_n(\theta'), \quad \eta(\theta, \theta') = \sum_n \sqrt{\Lambda_n} u_n(\theta) w_n^*(\theta'), \quad (14)$$

where  $\Lambda_n$  and  $\tilde{\Lambda}_n = \Lambda_n + 1$  are the eigenvalues and  $u_n(\theta)$  and  $w_n(\theta')$  the eigenfunctions. One can parameterize the eigenvalues as  $\Lambda_n = \sinh^2(r_n)$  and  $\tilde{\Lambda}_n = \cosh^2(r_n)$ , where the parameter  $r_n$  can be interpreted as a gain in mode  $n$ .

Using Eq. (13), we can calculate the angular intensity distribution:

$$\langle \hat{N}(\theta) \rangle = \langle [\hat{a}^{\text{out}}(\theta)]^\dagger \hat{a}^{\text{out}}(\theta) \rangle = \int d\theta' |\beta(\theta, \theta')|^2, \quad (15)$$

which, due to the orthogonality of the Schmidt modes, can be represented as the sum of the intensities of individual Schmidt modes:

$$\langle \hat{N}(\theta) \rangle = \sum_n \Lambda_n |u_n(\theta)|^2. \quad (16)$$

The gain  $G_2$  of the amplifier, which we measure from the pump power dependence of the mean photon number at zero angle,  $\langle \hat{N}^{\text{AV}}(\theta = 0) \rangle = \sinh^2(G_2)$ , is then related to the gain values of the Schmidt modes:

$$\langle \hat{N}^{\text{AV}}(\theta = 0) \rangle = \sum_n \Lambda_n |u_n(\theta = 0)|^2. \quad (17)$$

Using the Schmidt decomposition, we introduce the input and output broadband Schmidt operators:

$$\hat{A}_n^{\text{in}} = \int d\theta w_n^*(\theta) \hat{a}^{\text{in}}(\theta), \quad \hat{A}_n^{\text{out}} = \int d\theta u_n^*(\theta) \hat{a}^{\text{out}}(\theta). \quad (18)$$

We see that the input and output Schmidt operators are related to different eigenfunctions,  $w_n(\theta)$  and  $u_n(\theta)$ , respectively. Therefore, we will further call the set of functions  $w_n(\theta)$  *the input Schmidt modes*, while the functions  $u_n(\theta)$ , *the output Schmidt modes*. These eigenfunctions have the same absolute values but different phases. The phase difference is a consequence of the time-ordering effect, which is important in the high-gain regime [34], but can be neglected in the low-gain regime, where  $w_n(\theta) = u_n(\theta)$ .

Substituting the Schmidt decomposition (14) into the Bogoliubov transformation for the plane-wave operators (13), we obtain the input/output relations for the Schmidt operators,

$$\hat{A}_n^{\text{out}} = \sqrt{\Lambda_n + 1} \hat{A}_n^{\text{in}} + \sqrt{\Lambda_n} [\hat{A}_n^{\text{in}}]^\dagger, \quad (19)$$

while the inverse transformation reads

$$\hat{A}_n^{\text{in}} = \sqrt{\Lambda_n + 1} \hat{A}_n^{\text{out}} - \sqrt{\Lambda_n} [\hat{A}_n^{\text{out}}]^\dagger. \quad (20)$$

The output Schmidt operators of the first crystal (squeezer)  $\hat{A}_l$  can be decomposed over the input Schmidt operators of the second crystal (amplifier)  $\hat{A}_n^{\text{amp, in}}$ :

$$\hat{A}_l = \sum_n g_{ln} \hat{A}_n^{\text{amp, in}}, \quad (21)$$

where  $g_{ln} = \int d\theta [v_l(\theta)]^* w_n(\theta)$  are the overlap coefficients between the output modes  $v_l(\theta)$  of the squeezer and the input modes  $w_n(\theta)$  of the amplifier. Note that according to the Schmidt decomposition, both modes  $v_n(\theta)$  and  $w_n(\theta)$  form orthogonal sets, therefore  $\sum_n |g_{ln}|^2 = \sum_l |g_{ln}|^2 = 1$ .

Similarly, the output Schmidt operators of the amplifier  $\hat{A}_n^{\text{amp,out}}$  can be decomposed over the output Schmidt operators of the entire interferometer  $\hat{A}_k^{\text{int,out}}$ :

$$\hat{A}_n^{\text{amp,out}} = \sum_k h_{nk} \hat{A}_k^{\text{int,out}}, \quad (22)$$

where  $h_{nk} = \int d\theta [u_n^{\text{amp}}(\theta)]^* u_k(\theta)$  are the corresponding overlap coefficients with the normalization  $\sum_n |h_{nk}|^2 = \sum_k |h_{nk}|^2 = 1$ . Note that the output modes of the amplifier  $u_n^{\text{amp}}(\theta)$  coincide with the amplified vacuum modes mentioned in the main text.

Substituting Eq. (20) and Eq. (22) in Eq. (21), we find a connection between the output Schmidt operators of the squeezer and the output Schmidt operators of the entire interferometer:

$$\hat{A}_l = \sum_{n,k} g_{ln} \left[ \sqrt{\Lambda_n + 1} h_{nk} \hat{A}_k^{\text{int,out}} \mp \sqrt{\Lambda_n} h_{nk}^* \left[ \hat{A}_k^{\text{int,out}} \right]^\dagger \right], \quad (23)$$

where the “ $-$ ” sign corresponds to the positive gain of the amplifier (resulting in the bright fringe), while “ $+$ ” corresponds to the negative gain of the amplifier (resulting in the dark fringe).

**Funding.** This work was funded within the QuantERA II Programme (project SPARQL) that has received funding from the European Union’s Horizon 2020 research and innovation programme under Grant Agreement No 101017733, with the funding organization Deutsche Forschungsgemeinschaft. I. B., M. K., N. L., and M. C. are part of the Max Planck School of Photonics, supported by BMBF, Max Planck Society, and Fraunhofer Society. We acknowledge financial support of the Deutsche Forschungsgemeinschaft (DFG) via Project SH 1228/3-1 and via the TRR 142/3 (Project No. 231447078, Subproject No. C10). We also thank the PC2 (Paderborn Center for Parallel Computing) for providing computation time.

**Disclosures.** The authors declare no conflicts of interest.

**Data availability.** Data underlying the results presented in this paper are not publicly available at this time but may be obtained from the authors upon reasonable request.

## References

1. U. L. Andersen, T. Gehring, C. Marquardt, and G. Leuchs, Phys. Scr. 91 053001 (2016).
2. V. Giovannetti, S. Lloyd, and L. Maccone, Science 306, 1330-1336 (2004).
3. B.P. Abbott et al. (LIGO Scientific Collaboration and Virgo Collaboration), Phys. Rev. Lett. 119, 161101 (2017).
4. L. Barsotti, J. Harms, and R. Schnabel, Rep. Prog. Phys. 82 016905 (2019).
5. R. de Andrade, H. Kerdoncuff, K. Berg-Sørensen, T. Gehring, M. Lassen, and U. Andersen, Optica 7, 470-475 (2020).
6. G. Brida, M. Genovese, and I. Ruo Berchera, Nat. Photonics 4, 227 (2010).
7. C.A. Casacio, L.S. Madsen, A. Terrasson et al., Nature 594, 201–206. <https://doi.org/10.1038/s41586-021-03528-w>, (2021).
8. N. Samantaray, I. Ruo-Berchera, A. Meda, Light Sci. Appl. 6, e17005 (2017).
9. J. Roslund, R. de Araújo, S. Jiang et al., Nature Photon. 8, 109–112 (2014).
10. M. Chen, N. C. Menicucci, and O. Pfister, Phys. Rev. Lett. 112, 120505 (2014).
11. M. V. Larsen, X. Guo, C. R. Breum, J. S. Neergaard-Nielsen, U. L. Andersen, Science 366 (6463), • DOI: 10.1126/science.aay4354
12. Y. Cai, J. Roslund, G. Ferrini, F. Arzani, X. Xu, C. Fabre and N. Treps, Nat. Commun. 8, 15645 (2017).
13. L. La Volpe, S. De, T. Kouadou, D. Horoshko, M. I. Kolobov, C. Fabre, V. Parigi, and N. Treps, Opt. Express 28, 12385-12394 (2020).
14. A. M. Pérez, P. R. Sharapova, S. S. Straupe, F. M. Miatto, O. V. Tikhonova, G. Leuchs, and M. V. Chekhova Phys. Rev. A 92, 053861 (2015).
15. G. C. G. Berkhout, M. P. J. Lavery, J. Courtial, M. W. Beijersbergen, and M. J. Padgett, Phys. Rev. Lett. 105, 153601 (2010).

16. X. Gu, M. Krenn, M. Erhard, and A. Zeilinger, *Phys. Rev. Lett.* 120, 103601 (2018).
17. Y. Zhou, M. Mirhosseini, D. Fu, J. Zhao, S. M. H. Rafsanjani, A. E. Willner, and R. W. Boyd, *Phys. Rev. Lett.* 119, 263602 (2017).
18. V. Ansari, J. M. Donohue, M. Allgaier, L. Sansoni, B. Brecht, J. Roslund, N. Treps, G. Harder, and C. Silberhorn, *Phys. Rev. Lett.* 120, 213601 (2018).
19. Y. Shaked, Y. Michael, R. Z. Vered, L. Bello, M. Rosenbluh, and A. Pe'er, *Nat. Commun.* 9, 609 (2018).
20. G. Frascella, E. E. Mikhailov, N. Takanashi, R. V. Zakharov, O. V. Tikhonova, and M. V. Chekhova, *Optica* 6, 1233-1236 (2019).
21. N. Takanashi, A. Inoue, T. Kashiwazaki, T. Kazama, K. Enbutsu, R. Kasahara, T. Umeki, and A. Furusawa, *Opt. Express* 28, 34916-34926 (2020).
22. R. Nehra, R. Sekine, L. Ledezma, Q. Guo, R. M. Gray, A. Roy, and A. Marandi, *Science* 377, 1333-1337(2022).
23. U. Leonhardt, Cambridge University Press, *Measuring the quantum state of light* (1997).
24. G. Frascella, S. Agne, F. Ya. Khalili, and M. V. Chekhova, *npj Quantum Information* 7, 72 (2021).
25. M. A. Finger, N. Y. Joly, P. St. J. Russell, M. V. Chekhova, *Phys. Rev. A* 95, 053814 (2017).
26. L. Beltran, G. Frascella, A. M. Perez, R. Fickler, P. R. Sharapova, M. Manceau, O. V. Tikhonova, R. W. Boyd, G. Leuchs, and M. V. Chekhova, *J. Opt.* 19, 044005 (2017).
27. W. Wasilewski, A. I. Lvovsky, K. Banaszek, and C. Radzewicz, *Phys. Rev. A* 73, 063819 (2006).
28. A. Eckstein, and C. Silberhorn, *Opt. Lett.* 33, 1825-1827 (2008).
29. G. Patera, N. Treps, C. Fabre, G. J. de Valcárcel, *Eur. Phys. J. D* 56, 123 (2010).
30. V. A. Averchenko, G. Frascella, M. Kalash, A. Cavanna, and M. V. Chekhova, *Phys. Rev. A* 102, 053725 (2020).
31. S. L. Braunstein, *Phys. Rev. A* 71, 055801, (2005).
32. S. S. Straupe, D. P. Ivanov, A. A. Kalinkin, I. B. Bobrov, and S. P. Kulik, *Phys. Rev. A* 83, 060302(R) (2011).
33. G. Frascella, R. V. Zakharov, O. V. Tikhonova and M. V Chekhova, *Laser Phys.* 29, 124013 (2019).
34. A. Christ, B. Brecht, W. Mauerer, and C. Silberhorn, *New J. Phys.* 15, 053038 (2013).
35. P. R. Sharapova, G. Frascella, M. Riabinin, A. M. Pérez, O. V. Tikhonova, S. Lemieux, R. W. Boyd, G. Leuchs, and M. V. Chekhova, *Phys. Rev. Research* 2, 013371 (2020).
36. D. Scharwald, T. Meier, and P. R. Sharapova, *Phys. Rev. Research* 5, 043158 (2023)
37. M. Riabinin, P. R. Sharapova, and T. Meier, *Opt. Express* 29, 21876-21890 (2021)